Biological Trace Element Research (2024) 202:1288–1304
https://doi.org/10.1007/s12011-023-03738-5

RESEARCH

Enhanced Induction of Apoptosis and Cell Cycle Arrest in MCF-7 Breast Cancer and HT-29 Colon Cancer Cell Lines via Low-Dose Biosynthesis of Selenium Nanoparticles Utilizing *Lactobacillus casei*

Zahra Haji Mehdi Nouri[1] · Farzaneh Tafvizi[2] · Kumarss Amini[3] · Nooshin Khandandezfully[4] · Babak Kheirkhah[5]

Received: 16 February 2023 / Accepted: 18 June 2023 / Published online: 1 July 2023

Abstract

As a leading global cause of mortality, cancer continues to pose a significant challenge. The shortcomings of prevalent cancer treatments, such as surgery, radiation therapy, and chemotherapy, necessitate the exploration of alternative therapeutic strategies. Selenium nanoparticles (SeNPs) have emerged as a promising solution, with their synthesis being widely researched due to their potential applications. Among the diverse synthesis methods for SeNPs, the green chemistry approach holds a distinctive position within nanotechnology. This research delves into the anti-proliferative and anticancer properties of green-synthesized SeNPs via the cell-free supernatant (CFS) of *Lactobacillus casei* (*LC*-SeNPs), with a specific focus on MCF-7 and HT-29 cancer cell lines. SeNPs were synthesized employing the supernatant of *L. casei*. The characterization of these green-synthesized SeNPs was performed using TEM, FE-SEM, XRD, FT-IR, UV–vis, energy-dispersive X-ray spectroscopy, and DLS. The biological impact of *LC*-SNPs on MCF-7 and HT-29 cancer cells was examined via MTT, flow cytometry, scratch tests, and qRT-PCR. Both FE-SEM and TEM images substantiated the spherical shape of the synthesized nanoparticles. The biosynthesized *LC*-SNPs reduced the survival of MCF-7 (by 20%) and HT-29 (by 30%) cells at a concentration of 100 µg/mL. Flow cytometry revealed that *LC*-SNPs were capable of inducing 28% and 23% apoptosis in MCF-7 and HT-29 cells, respectively. In addition, it was found that *LC*-SNPs treated MCF-7 and HT-29 cells were arrested in the sub-G1 phase. Gene expression analysis indicated that the expression levels of the *CASP3*, *CASP9*, and *BAX* genes were elevated after treating MCF-7 and HT-29 cells with *LC*-SNPs. Further, SeNPs were observed to inhibit migration and invasion of MCF-7 and HT-29 cancer cells. The SeNPs, produced via *L. casei*, demonstrated strong anticancer effects on MCF-7 and HT-29 cells, suggesting their potential as biological agents in cancer treatment following additional in vivo experiments.

Keywords Apoptosis · Anti-breast cancer · Anti-colon cancer · Green synthesis · *Lactobacillus casei* · Selenium nanoparticles

Introduction

Cancer ranks as the second most common cause of death globally, surpassed only by cardiovascular diseases [1]. In 2020, global cancer rates were estimated at 19.3 million cases, resulting in approximately 10 million deaths [2]. Women worldwide express a significant concern about malignancies, with breast cancer being the most prevalent, constituting about 25% of all gynecological cancers [3, 4]. Various treatment methods such as surgery, chemotherapy,

✉ Farzaneh Tafvizi
Farzaneh.Tafvizi@iau.ac.ir; farzanehtafvizi54@gmail.com

Zahra Haji Mehdi Nouri
zahra.nouri@ymail.com

Kumarss Amini
dr_kumarss_amini@yahoo.com

Nooshin Khandandezfully
nooshinkhandan22@gmail.com

Babak Kheirkhah
Babakkheirkhah@yahoo.com

[1] Department of Cellular and Molecular Biology, Sirjan Branch, Islamic Azad University, Sirjan, Iran

[2] Department of Biology, Parand Branch, Islamic Azad University, Parand, Iran

[3] Department of Microbiology, School of Basic Science, Saveh Branch, Islamic Azad University, Saveh, Iran

[4] Faculty Member, Department of Microbiology, Sirjan Branch, Islamic Azad University, Sirjan, Iran

[5] Department of Microbiology, Faculty of Veterinary Medicine, Baft Branch, Islamic Azad University, Baft, Iran

radiation therapy, and monoclonal antibodies are selected based on the patient's specific circumstances. Nevertheless, the current treatments' limitations in efficacy and safety necessitate the exploration of novel technologies to develop more effective treatment alternatives [5, 6].

Colorectal cancer (CRC), accounting for 10% of all cancers, holds the third position in the global cancer prevalence hierarchy and is implicated in a substantial portion of cancer-related fatalities [7]. Multiple treatment options for CRC, including surgery, chemotherapy, radiation therapy, and palliative care, are currently available [8]. Although traditional treatments can eliminate cancer cells, they also inadvertently harm healthy cells. Consequently, the quest for innovative treatment strategies has stimulated the invention and progression of novel cancer therapies [6].

In recent years, nanotechnology has made significant advances, especially in the creation of various medications. The production of nanoparticles represents a significant achievement in the effective diagnosis and treatment of diverse diseases. The manufacturing of nanoparticles employs biological materials such as microorganisms, enzymes, cells, and plant extracts [9]. There has been a marked increase in interest in deploying biogenetically engineered metallic nanoparticles (NPs) for cancer theranostics. The biological synthesis of nanoparticles, using organisms such as bacteria, actinomycetes, fungi, and plants, has been explored as a simpler and more cost-effective alternative to other chemical and physical methods [10]. Recently, considerable attention has been given to nanoparticle synthesis through green methods, using plants and bacteria, due to its numerous advantages [11, 12]. One such advantage is that the green synthesis of nanoparticles eliminates the need for cell cultures, which are labor-intensive and expensive, thereby increasing scalability and industrial applicability [13].

The unique characteristics of nanoparticles have recently sparked interest in utilizing microbial strains for nanoparticle synthesis. The distinct physicochemical properties of nanomaterials, compared to their non-nano counterparts, have stimulated extensive research in this field over the past few decades [14, 15]. Organisms have developed sophisticated mechanisms to survive in environments with high concentrations of undesirable ions, including transforming the chemical nature of a toxic ion into a non-toxic form, ultimately leading to the formation of corresponding nanoparticles [16]. Therefore, nanoparticles can be considered a byproduct of an organism's resistance mechanism to a particular ion [17].

Selenium (Se) is a vital element that has garnered the attention of numerous researchers owing to its unique physicochemical and electrical characteristics [18]. This crucial micronutrient, found in a variety of sources such as organ meats, seafood, plants, cereals, and nuts, is integral to human health [19]. Its distinctive properties and potential uses in the realms of physics, chemistry, and biology have been widely acknowledged [20, 21]. As a trace element fundamental to all forms of life, selenium constitutes a component of selenocysteine in many enzymes, making it indispensable to all living beings [22]. In humans, selenium serves as a coenzyme for glutathione peroxidases and thioredoxine reductases, playing a vital role in the development of the immune system, cancer prevention, and antioxidant and antiviral effects [23]. Selenium nanoparticles (SeNPs), with their unique optical, electronic, electrocatalytic, and biological properties, carry considerable potential for technology applications across diverse fields, including medicine, diagnosis, therapy, electronic devices, catalysis, and chemical sensors [24].

SeNPs exhibit an array of biological attributes, such as antioxidant [25] and antimicrobial effects [26], immune system regulation [27], and tumor prevention [28]. As such, SeNPs have been identified as a key type of nanoparticle in medical research [29, 30]. Studies have shown that SeNPs have less toxicity and display superior biological activity when compared to common forms of selenium, such as se^{+4} and se^{+6} ions [31, 32]. Hence, SeNPs have been employed as a new addition to drug nanocarriers for drug delivery systems, particularly as selenium is a necessary dietary micronutrient in the form of SeNPs [33]. When scaled to the nanolevel, selenium functions as a promising chemo-preventive agent with lower toxicity [34, 35]. Several mechanisms of SeNPs' anticancer effects have been identified, including the production of reactive oxygen species (ROS), activation of apoptotic pathways, mitochondrial dysfunction, DNA fragmentation, cell cycle arrest, and disruption of cellular homeostasis, [36–39]. In the study at hand, we synthesized SeNPs using *Lactobacillus casei* (*LC*-SeNPs) cell-free supernatant to assess their anticancer effects on MCF-7 breast cancer and HT-29 colon cancer cell lines.

Material and Method

Reagents

Sodium selenite (Na_2SeO_3), RPMI-1640 medium, fetal bovine serum (FBS, courtesy of DENAzist Asia's Co), and penicillin–streptomycin (PS) 100 X were all procured from Gibco, ThermoFisher Scientific (Waltham, MA, USA). MTT [3-(4,5-dimethyl-2-thiazolyl)-2,5-diphenyl-2-H-tetrazolium bromide] and DMSO (dimethyl sulfoxide) were sourced from Merck (Germany). The Annexin V-FITC kit and 2′-7′-dichlorodihydrofluorescein diacetate (DCFHDA) were obtained from Roche (Munich, Germany). Ultra-pure water was generated using Milli-Q (Millipore, Darmstadt, Germany). DAPI (4′,6-diamidino-2-phenylindole dihydrochloride) was purchased from Sigma-Aldrich (St. Louis, MO, USA).

Preparation of Supernatant and Production of *LC*-SeNPs

The *L. casei* (Strain 6904) required for the synthesis of selenium nanoparticles was procured from the Iranian Biological Resources Center (IBRC). Initially, the selected strain was grown in 50 mL de Man, Rogosa, and Sharpe (MRS) (Merck Millipore) liquid culture medium in a shaker incubator at 30 °C, with a speed of 150 rpm, over 18 h. Following this, 1 mL of the cultured *L. casei* was introduced to 100 mL MRS liquid culture medium (1% V/V), and the mixture was incubated at the same conditions for 72 h. The culture supernatant, after 72 h, was collected via centrifugation at 6000 rpm (Hettich, Germany) at room temperature for 20 min. This supernatant was then condensed using a freeze dryer (Alpha 1–2 LDPlus, Christ, Germany) until the volume reduced to 30 mL. This concentrated supernatant was then employed in the synthesis of *LC*-SeNPs. *LC*-SeNPs were produced by slightly modifying the protocol established by Xu et al. [40]. To summarize, 4 mM of Na_2SeO_3 was dissolved in 10 mL of distilled water, followed by the addition of 10 mL of bacterial supernatant, and the mixture was stirred at 40 °C for 3 h and 350 rpm. The emergence of an orange color indicated successful formation of selenium nanoparticles. The precipitate was rinsed with distilled water, then subjected to 10-min centrifugation at 13,000 rpm (Eppendorf 5804R, Germany) three times, and the final product was left to dry in the incubator.

Characterization of the Produced *LC*-SeNPs

Post-production, the structure, and morphology of the synthesized nanoparticles were confirmed using a variety of methods, such as ultraviolet–visible spectroscopy (UV–vis) (UV 1601, Shimadzu), field emission scanning electron microscopy (SEM) (Zeiss, Sigma VP model), energy-dispersive X-ray spectroscopy (EDX) (Zeiss, Sigma VP model), transmission electron microscopy (TEM) (Leo 906, Zeiss100KV model, Germany), X-ray powder diffraction (XRD) (PANalytical's X′Pert PRO MRD), and Fourier transform infrared spectroscopy (FT-IR) (Spectrum Two FT-IR Spectrometer (Perkin Elmer)). Dynamic light scattering particle size distribution analysis (DLS) and zeta potential of *LC*-SeNPs were determined by Malvern Instruments Nano Zetasizer (Worcestershire, UK). The characterization tests were conducted as per our earlier study [41].

Cell Culture

Cell lines of HT-29, MCF-7, and human foreskin fibroblasts (HFF) were purchased from the Pasture Institute Cell Bank in Iran, Tehran. The cells were grown in RPMI 1640 medium (Gibco, USA) that was supplemented with 1% (V/V) penicillin–streptomycin and 10% heat-inactivated FBS, and 2 mM L-glutamine. The cells were kept in a 5% CO_2 incubator at 37 °C.

Assessment of *LC*-SeNP Cytotoxicity via MTT Assay.

The MTT assay was utilized to evaluate the cytotoxic impact of *LC*-SeNPs on the HT-29 and MCF-7 cell lines. Initially, the cells (1×10^4 cells/well) were seeded. Subsequently, HT-29 and MCF-7 cancer cells were exposed to varying concentrations of the *LC*-SeNPs (3.125, 6.25, 12.5, 25, 50, and 100 mg/mL) at 24-, 48-, and 72-h intervals at 37 °C and 5% CO_2. After incubation, 20 µL of MTT dye solution was added to each well, and the plates were incubated for 24 h. The MTT dye was then removed, and 100 µL of DMSO was added to each well. Ultimately, the absorbance of the microwells was measured at 570 nm using the ELISA reader. This entire process was repeated thrice, along with the control group, and the IC_{50} value was determined using the obtained OD values as per the formula given in reference [12].

$$\text{Cell viability}(\%) = (\text{Abs test cells}/\text{Abs control cells}) \times 100$$

Flow Cytometry Assessment of Apoptosis

Apoptotic induction was detected in HT-29 and MCF-7 cells (10^5 cells/well), treated with IC_{50} concentration of *LC*-SeNPs for a duration of 24 h, as per the guidelines provided in the Annexin V-FITC kit (eBioscience, Affymetrix, USA) manual. The stained cells' analysis was conducted using a flow cytometry apparatus (Biocompare, USA). For comparison, untreated HT-29 and MCF-7 cells were utilized as a baseline control [42].

DAPI Staining

The DAPI staining protocol is employed to assess apoptosis in HT-29 and MCF-7 cells exposed to *LC*-SeNPs. The cells are initially seeded in 6-well plates before treating with an IC_{50} concentration of *LC*-SeNPs for 24 h and fixation with 0.4% formaldehyde. Following fixation, the cells are stained with 0.5 mg/mL DAPI dye for 5 min at ambient temperature. Afterward, the cells are thoroughly rinsed twice with PBS and inspected under the Olympus IX81 inverted fluorescence microscope (Olympus, Hamburg, Germany). Apoptosis is ultimately deduced from the detected nuclear fragmentation [43].

Apoptotic Genes Expression via qRT-PCR

The relative expression of apoptotic genes, namely, BCL2-associated X (*BAX*), BCL2 apoptosis regulator (*BCL2*), Caspase 3 (*CASP3*), and Caspase 9 (*CASP9*), is determined through qRT-PCR.

Initially, total RNA from treated and untreated cells is extracted following the instructions of an RNA extraction kit (CinnaGen, Iran). The extracted RNA's quality and quantity are then verified using a nanodrop (IMPLEN GMBH). This is followed by cDNA synthesis using the Revers AidTM First Strand cDNA Synthesis Kit (Fermentas, USA). The expression of *BAX*, *BCL2*, *CASP3*, and *CASP9* genes is then scrutinized using qRT-PCR on a Light Cycler (Bioneer, Daejeon, Korea), with beta-actin (*ACTB*) employed as an internal control.

The cDNA synthesis involves the addition of 3 µg of total RNA to a blend containing 1 µL of 10×buffer and 1 µL of DNAse, incubated at 37 °C for 30 min. Afterward, 1 µL EDTA is added and further incubated at 65 °C for 30 min to inhibit DNAse activity. A mixture of 4 µL of 5×buffer, 1.5 µL of MgCl2, 2 µL of dNTP mix (10 mM), 2 µL of random hexamer primer, 0.5 µL of RNasin (40 Unit/µL), and 1 µL of reverse transcriptase (RT) enzymes is then prepared and incubated at 42 °C for 60 min. Finally, the RT enzyme is deactivated by heating at 70 °C for 10 min.qRT-PCR reactions are set up in a final volume of 20 µL, comprising 10 µL master mix (Bioneer, South Korea), 1 µL of each primer (10 mM) (Table 1), 1 µL of cDNA, and 8 µL of PCR-grade H2O. The thermal cycling parameters consist of initial DNA denaturation at 95 °C for 1 min, followed by 40 cycles of 95 °C for 20 s, 62 °C for 40 s, and 72 °C for 10 s. The relative change in gene expression for all genes, compared to the *ACTB* control gene, is calculated using the widely accepted $2^{-\Delta\Delta Ct}$ method [41, 42].

Cell Cycle Assay

HT-29 and MCF-7 cell lines were cultured in 6-well plates (10^6 cells/well) and treated with a half maximal inhibitory concentration (IC_{50}) of *LC*-SeNPs for a period of 24 h. Subsequent to the treatment, cells were rinsed twice with PBS and underwent centrifugation at 1500 rpm for 5 min. Thereafter, cells were stained with 250 mL of propidium iodide (PI) dye and incubated for half an hour. A second round of centrifugation was then conducted at 5000 rpm for 5 min at room temperature. The cell cycle stages were identified using a BD FACScan Cell Flow Cytometer (Becton Dickinson, USA). The outcomes were conveyed as the percentage representation of cells in each phase of the cell cycle using the Flow Jo software (Version 7.6.1) [12].

Cellular Uptake of *LC*-SeNPs.

On 6-well culture plates, 1×10^5 MCF-7 cancer cells were seeded, and the plates were incubated for 24 h at 37 °C in 5% CO_2. The cells were treated with IC_{50} concentration of *LC*-SeNPs and Cy7 dye (7 µg/mL) for 24 h. Then, the cells were trypsinized, transported to tubes, and centrifuged after being washed three times with PBS to remove the free nanoparticles. For quick examination, the pellets were re-suspended in 0.5 mL of PBS, fixed in 4% paraformaldehyde, and stained with DAPI. At last, the fluorescence amplitude of each well was determined using a microplate reader (Biotek Synergy HT, USA) with an excitation wavelength of 750 nm and an emission wavelength of 775 nm. Becton Dickinson's Cell Quest software was used to gather and evaluate data from 1×10^4 cells. A confocal laser-scanning microscope (A1, Nikon, Switzerland) was used to detect the cellular uptake of *LC*-SeNPs [44].

Wound Healing Assay

Cancer cells under growth were subjected to trypsinization, and 2×10^5 cells were dispensed per well in a 12-well plate, followed by a 24-h incubation period. Once 90% cell confluency was achieved, a scratch was introduced via a 200-µL sterile pipette tip to create a cell-free zone. Cellular debris was then eliminated with a gentle wash using culture medium, and initial images were captured (0 h). The HT-29 and MCF-7 cells were left to invade for 24 h, and the impact of nanoparticles on wound healing was evaluated at the conclusion of the 24-h incubation period via secondary microscopy. The progress of wound closure was analyzed using the Image-J 1.45 software [45].

Table 1 Primer characteristics of target genes

Genes	Reverse or forward	Primer sequences	Size (bp)	Tm (°C)	Length of PCR product
BAX	F	5′-ATGTTTTCTGACGGCAACTTC-3	21	55	133 bp
	R	5′-AGTCCAATGTCCAGCCCAT-3′	19		
BCL2	F	5′-ATGTGTGTGGAGACCGTCAA-3′	20	65	141 bp
	R	5′-GCCGTACAGTTCCACAAAGG-3′	20		
CASP3	F	5′-TGTTTGTGTGCTTCTGAGCC-3′	20	60	210 bp
	R	5′-CACGCCATGTCATCATCAAC-3′	20		
CASP9	F	5′-CATTTCATGGTGGAGGTGAAG-3′	21	65	149 bp
	R	5′-GGGAACTGCAGGTGGCTG-3′	18		

Analysis of Statistical Data

The GraphPad Prism 8.0.2 software was utilized for statistical analysis. Quantitative data were expressed as mean ± standard deviation (SD), while qualitative information was represented as a percentage. The collected data were then examined using *t*-test, one-way and two-way analysis of variance (one-way ANOVA), with a $P < 0.05$ indicating a statistically significant disparity.

Results and Discussion

Physiochemical Characterization of *LC*-SeNPs Produced Through Eco-friendly Synthesis

The spherical form of *LC*-SeNPs was affirmed by the visual evidence provided by TEM and FE-SEM images (Fig. 1 A and B) [46]. The EDX spectrum showed a high Se peak at 1.4 keV (64.6%), suggesting the preferred purity of Se in the synthesized *LC*-SeNPs. In our research, we observed O (6.5%) and C (28.9%) peaks in the EDX graph encircling the *LC*-SeNPs (Fig. C).

The protein molecules probably involved in capping the synthesized nanoparticles are suggested by the detection of carbon and oxygen peaks. This inference is in line with prior characterization studies of SeNPs synthesized with the use of *Streptomyces minutiscleroticus*, *Pseudomonas aeruginosa* ATCC 27853, and *Bacillus mycoides* [47–49].

DLS analysis provided data on the size distribution and the polydispersity index (PDI) of SeNPs (Fig. 1D) [50]. SeNPs had an average size of 90.78 nm and a PDI of 0.28 (Fig. 1D).

Earlier studies have noted a range of sizes for SeNPs produced through bacterial mediation. These sizes were observed using various bacterial strains, including *Lactobacillus casei* ATCC 393 (spherical shape, 50–80 nm), *Escherichia coli* (spherical shape, 60 nm), and *Streptomyces bikiniensis* strainess_ama-1 (spherical shape, 50–100 nm) [40, 51, 52].

The *LC*-SeNPs displayed a zeta potential of -17.30 ± 0.56 mV, indicating satisfactory stability (Fig. 1E). The charge distribution on the *LC*-SeNPs can be assessed by the zeta potential, which can forecast the stability of colloidal SeNPs [53]. This observed event could be due to the inherent capping of the nanoparticles by biomolecules, providing an additional advantage in environmentally friendly biosynthesis [54].

UV–vis spectroscopy verified the existence of SeNPs, formed through the reduction of selenium ions to elemental *LC*-SeNPs, with a peak observed at approximately 269 nm (Fig. 2A) [55, 56].

Further, XRD analysis was used to determine the crystallinity of SeNPs [57]. The XRD diffractogram demonstrated the creation of SeNPs, courtesy of the bacterial supernatant reducing agents, which led to the reduction of selenium. The XRD pattern of the synthesized

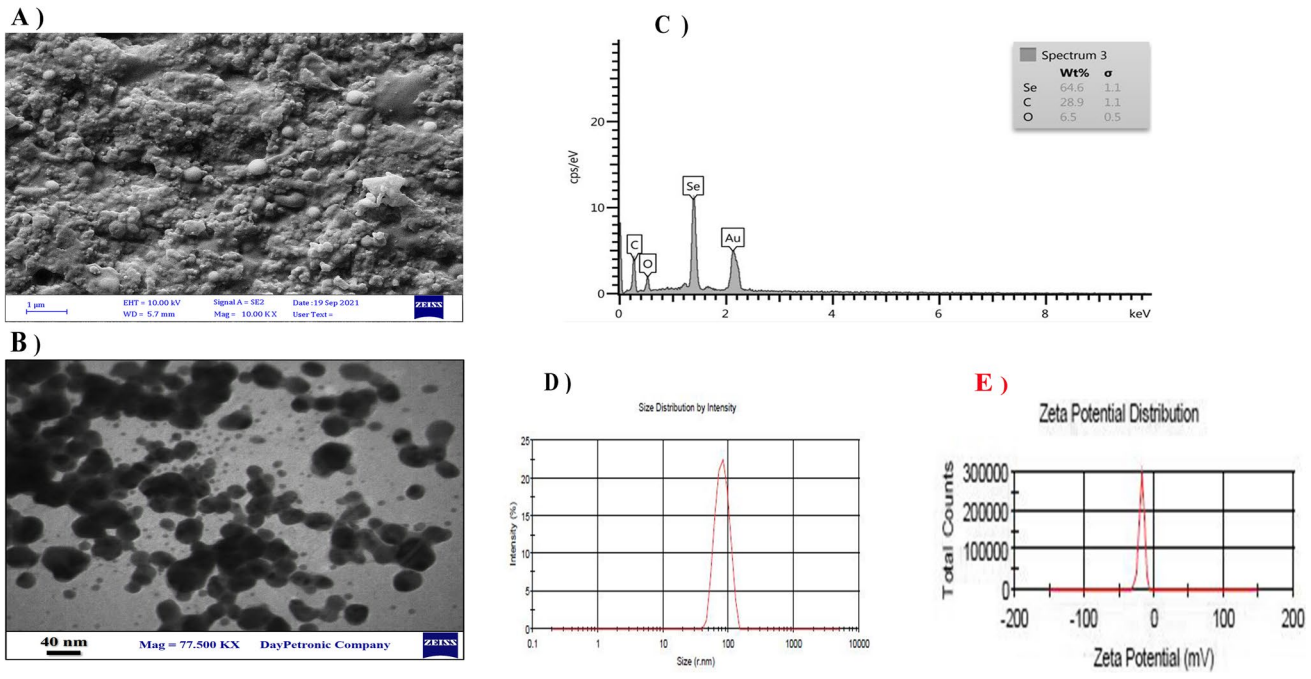

Fig. 1 SEM (**A**) and TEM (**B**) micrograph of biosynthesized SeNPs; EDX spectrum (**C**); DLS analysis (**D**) and ζ-potential of the of biosynthesized SeNPs (**E**)

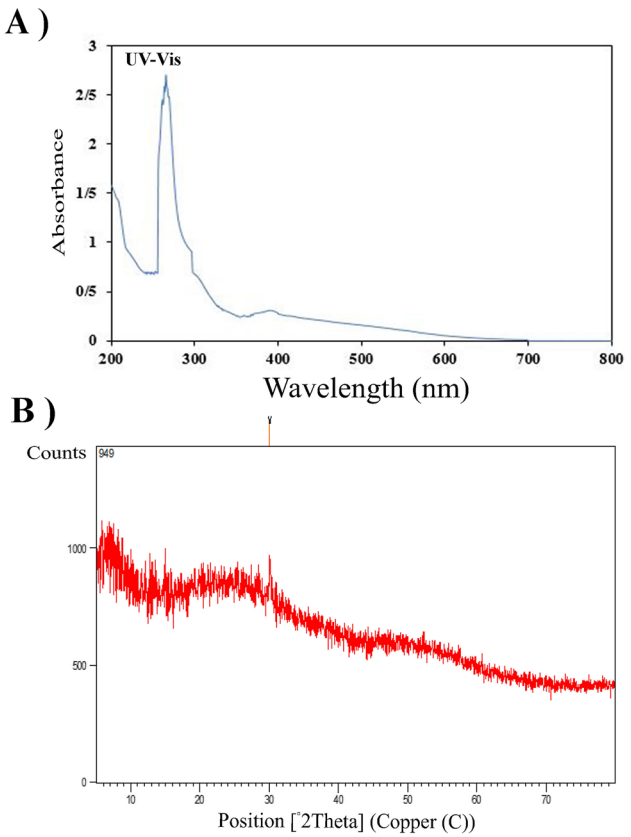

Fig. 2 UV–visible absorption spectrum (**A**) and X-ray diffraction spectra (**B**) of SeNPs synthesized using *Lactobacillus casei* extract

selenium SeNPs revealed a broad diffraction peak at lower angles, confirming their amorphous or non-crystalline state. This finding was noted in the 2B dataset. A peak index of 30.06° is associated with the crystalline metal structure of SeNPs (Fig. 2B).

The lack of additional pronounced selenium peaks, coupled with the broadening observed in the existing diffractogram, can be attributed to the binding of bacterial supernatant biomolecules to *LC*-SeNPs. This correlation brings about a loss of crystallinity, resulting in the formation of an amorphous selenium structure. This outcome concurs with previous scientific endeavors focused on the eco-friendly fabrication of SeNPs [58–60]. Moreover, the FT-IR spectrometry of bacterial supernatant was used in the green synthesis of SeNPs to identify the specific biomolecules involved in the reduction and capping of SeNPs [61]. Various biomacromolecules, predominantly proteins, have been found to participate in the reduction of selenite and selenate, leading to the stabilization of these compounds into SeNPs [54].

FT-IR spectrometry displayed a prominent and extensive peak at 3434 cm^{-1}, linked to the tensile absorption of O–H and N–H groups found in polysaccharide compounds and amino groups in bacterial proteins. The broad peak was a result of peak interferences related to the supernatant components, which included the absorption of C-H tensile vibrations connected with the alkene compounds' double bonds above 3000 cm^{-1}. The absorption peak of C = O and C-N bonds in the nucleotides and nitrogenous compounds of supernatant protein prominently appeared at 1618 cm^{-1} and 1381 cm^{-1}, respectively. The tensile vibration frequencies related to C-O–H and C–O–C bonds of polysaccharide compounds were faintly visible at 1000 cm^{-1}. Off-plane bending vibrations associated with C = C-H bonds were exhibited at 617 and 995 cm^{-1} (Fig. 3A).

In the FT-IR spectrum of reduced SeNPs, the presence of several peaks is associated with the coating of SeNPs by diverse molecules. The absorption peak is related to the tensile vibrations of the O–H and N–H groups of polysaccharides and amino groups, which are broadly due to the peak overlap around 3437 cm^{-1}. The tensile vibrations absorption of the C-H aliphatic bonds of polysaccharide compounds at 2922 cm^{-1}, absorption of the carbonyl group C = O of proteins and nucleotides at 1625 cm^{-1}, the absorption peak of the C-N bond of nitrogenous compounds at 1362 cm^{-1}, C-O bond of polysaccharide derivatives at 1003 cm^{-1}, tensile vibrations of the C-O ester group of fats or phospholipids at 1264 cm^{-1}, and the absorption peak of the tensile vibration of the Se-O bond observed on the surface of SeNPs at 492 cm^{-1} were also detected. The shift at the tensile absorption peak of the C = O bond from 1618 to 1625 cm^{-1} compared to the initial spectrum could be connected to the binding of the supernatant organic compounds to the SeNPs' surface (Fig. 3B) [62]. The results of this study highlight the biosynthesis and stabilization of SeNPs through the involvement of bacterial proteins and metabolites [63].

In Vitro Cytotoxicity of *LC*-SeNPs

The MTT assay was used to determine the cytotoxicity and cell viability of *LC*-SeNPs. The study demonstrated a notable decrease in the survival rates of HT-29 and MCF-7 cells when exposed to all concentrations of *LC*-SeNPs, in contrast to the control group. The most significant drop in cell survival was observed at the 100 µg/mL concentration of *LC*-SeNPs ($P < 0.0001$). Additionally, a marked variation in the viability of HT-29 and MCF-7 cells was detected across concentrations of 12.5, 25, 50, and 100 µg/mL (Fig. 4A). Interestingly, MCF-7 cells exhibited substantially lower survival compared to HT-29 cells. The estimated IC_{50} values of *LC*-SeNPs for MCF-7 and HT-29 cells were 15.72 and 32.37 µg/mL, respectively (Fig. 4B). A significant difference in the IC_{50} values of *LC*-SeNPs was discerned after 24 h ($P < 0.01$) (Fig. 4C). These findings suggest that as the concentration of *LC*-SeNPs escalated, the survival rate of cancer cells diminished.

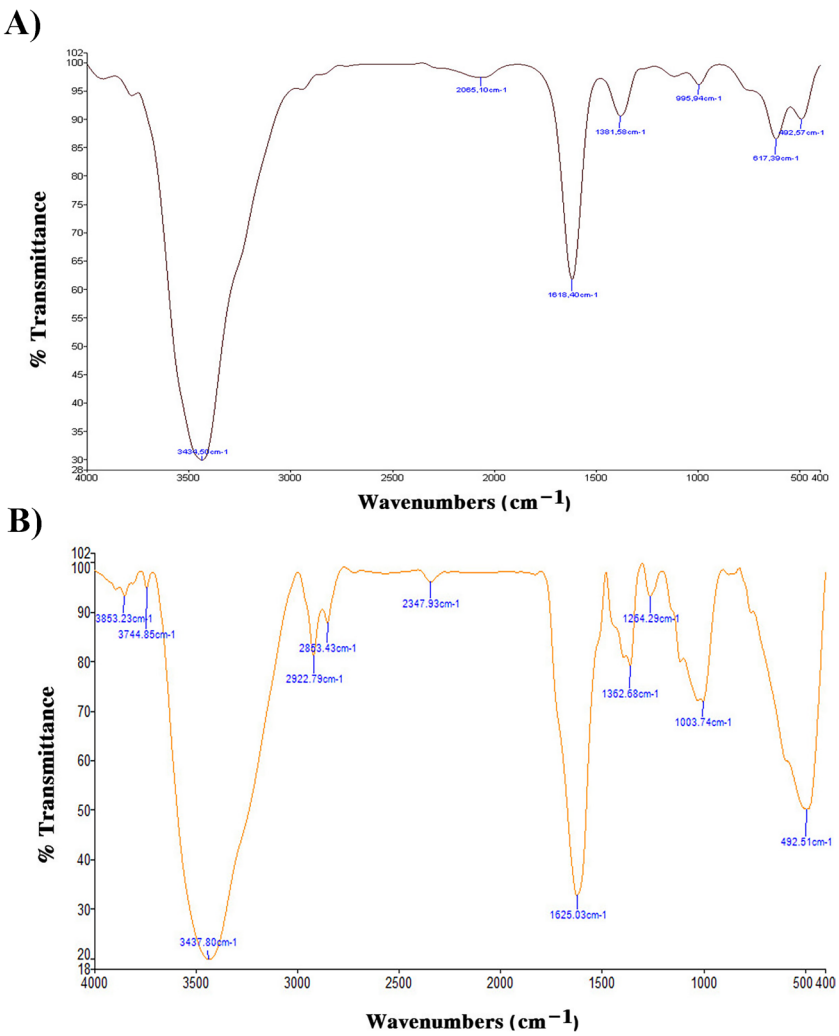

Fig. 3 Fourier transform infrared spectroscopy spectra of *Lactobacillus casei* extract (**A**) SeNPs synthesized using *Lactobacillus casei* extract (**B**)

Green synthesized *LC*-SeNPs exerted a far lesser impact on normal HFF cells compared to the HT-29 and MCF-7 cancer cells (Fig. 4D). MTT assay demonstrated more than 70% cell viability for HFF cells after treatment with a 100-µg/mL concentration of *LC*-SeNPs. The IC_{50} value of *LC*-SeNPs for HFF cells was calculated as 738 µg/mL. The outcomes indicated a very low toxicity of *LC*-SeNPs against HFF cells, thus attesting their biocompatibility. The cytotoxic effect of *LC*-SeNPs on cancer cells aligns with the findings of other studies, reaffirming our results [64, 65].

The uptake and cytotoxicity of metallic nanoparticles (NPs) within cells are influenced by several factors including their size, shape, concentration, the materials coating them, surface charge, and surface functionalization. Furthermore, the method of biosynthesis of metallic NPs, particularly when derived from natural sources, significantly impacts their bioactivity. A variety of biomolecules are involved in microbial synthesis, which act as capping agents during biosynthesis procedures [66]. Numerous research findings have highlighted the exceptional ability of SeNPs to cause cytotoxicity in cancer cells via multiple molecular and cellular mechanisms. These include cell cycle disruption, oxidative stress, mitochondrial damage, DNA destruction, and apoptosis initiation [67].

Recent investigations have revealed that the cellular membrane has a crucial role in the toxicity induced by *LC*-SeNPs in cancerous cells. SeNPs are found to alter the biomechanical characteristics of cancer cells, notably leading to a marked decrease in adhesion force and Young's modulus [30, 68].

Tabibi et al., through their examination of the anticancer effects of SeNPs on MCF-7 and HT-29 cell lines, revealed that a 100-µM concentration of SeNPs inhibited more than 75% of cancer cell growth [69]. Ranjitha et al. also reported potent cytotoxic activity of synthesized SeNPs against the HT-29 cell line, showing 40.5%, 33%, and 23.7% of cell viability at 2 µg/mL, 4 µg/mL, and 30 µg/mL concentrations, respectively [70].

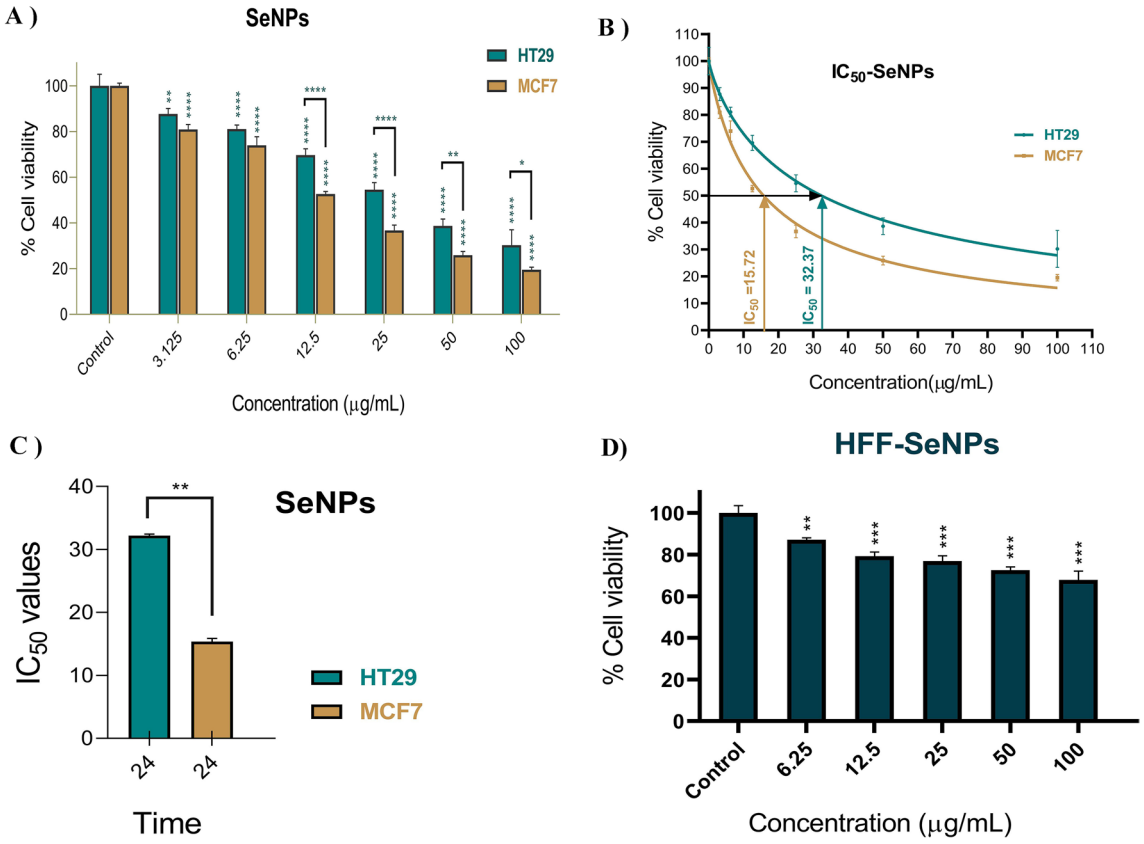

Fig. 4 Comparison of the cell viability percentage of MCF-7 and HT-29 cells treated with different concentrations (3.125, 6.25, 12.5, 25, 50, and 100 mg/mL) of *LC-SeNPs* compared to the control group (**A**). Comparison of the IC_{50} values of cells treated with different concentrations (**B**). Comparison of the difference between the IC_{50} values of *LC-SeNPs* in MCF-7 and HT-29 after 24 h (**C**). Investigation of the cell viability percentage of normal human foreskin fibroblast (HFF) cells treated with different concentrations of *LC-SeNPs* compared to the control group (**D**). (****$P<0.0001$, ***$P<0.001$, **$P<0.01$, and *$P<0.05$). The results are expressed as mean SD of three independent experiments ($n=3$)

Wadhwani et al. reported that SeNPs, synthesized using *Acinetobacter* sp.sW30, resulted in 53.5%, 26.6%, and 77% cell viability at a concentration of 100 µg/mL against 4T1, MCF-7, and HEK293 cells, respectively [71]. Biosynthesized SeNPs, using *Idiomarina* sp.PR58-8, exhibited a dose-dependent cytotoxicity against HeLa cells, with only 3% viability observed at a concentration of 100 µg/mL. No toxicity was detected against HaCaT normal cells [72].

Biogenic SeNPs, synthesized using *Streptomyces minutiscleroticus* M10A62, led to 99.5% and 100% cytotoxicity against HepG2 and HeLa cells [47].

The IC_{50} values of SeNPs, synthesized by *Streptomyces bikiniensis* strainess_ama-1, were found to be 75.96 µg/mL for HepG2, and 61.86 µg/mL for MCF-7 cancer cells [52].

A significant death rate in MCF-7cancer cells was noted following the treatment with SeNPs synthesized using *Bacillus* sp. MSh-1 (IC_{50}: 41.5 ± 0.9 µg/mL) [73].

Comparing IC_{50} values, it was clear that the *LC*-SeNPs in this study demonstrated potent antiproliferative activity against MCF-7 and HT-29 cancer cells, as compared to other green synthesized SeNPs.

LC-SeNPs Triggered Apoptosis in MCF-7 and HT-29 Cells

In the conducted research, the analysis via flow cytometry revealed the cytotoxic influence of *LC*-SeNPs resulted in both early and late stages of apoptosis in MCF-7 and HT-29 cells. Upon evaluation of the data, it was observed that 66% of MCF-7 and 73% of HT-29 cells remained viable. Notably, early apoptosis was evident in 10% of HT-29 and 14% of MCF-7 cells, while 13% of HT-29 and 14% of MCF-7 cells were in late apoptosis. Additionally, necrosis was found in 4% of HT-29 and 5% of MCF-7 cells. The results highlighted a notably high toxicity of *LC*-SeNPs towards the MCF-7 and HT-29 cancer cells ($P<0.0001$) (Fig. 5).

As depicted in Fig. 6, DAPI staining was performed on MCF-7 and HT-29 cells. Treated MCF-7 and HT-29 cancer cells displayed bright blue fluorescence with higher intensity

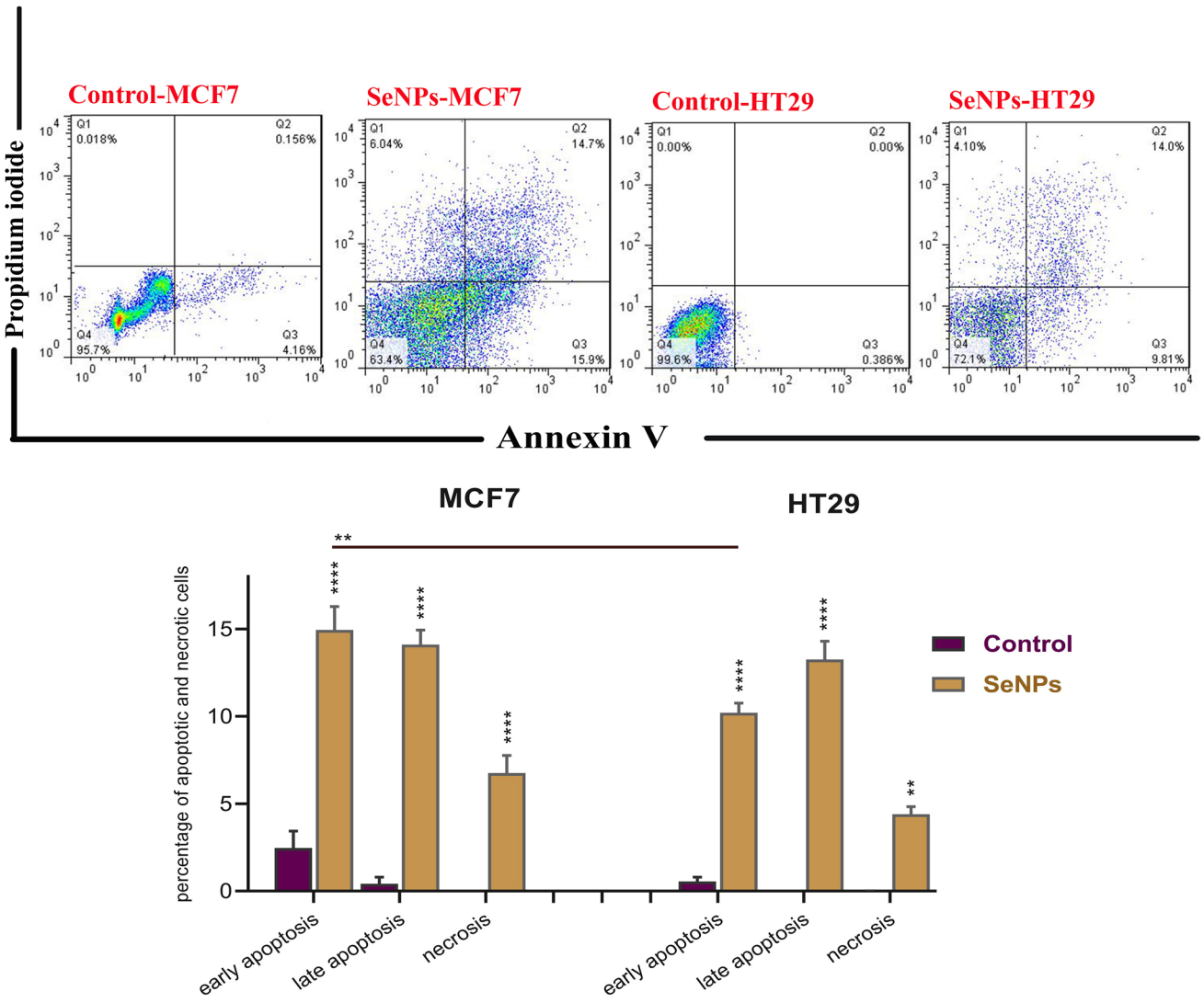

Fig. 5 Flow cytometry plot to evaluate apoptosis induced by *LC*-SeNPs on the MCF-7, HT-29, and control cells after 24 h (****$P < 0.0001$ and **$P < 0.01$)

compared to control-untreated cells. The untreated cells had a round shape. The nuclei stained homogeneously with less bright blue fluorescence. A pronounced blue fluorescence, a result of nuclear chromatin condensation, was noted in treated MCF-7 and HT-29 cells compared to those that were untreated. The condensation patterns of chromatin in the cell nuclei treated with *LC*-SeNPs provided evidence of apoptosis in MCF-7 and HT-29 cancer cells (Fig. 6). In accordance with previous findings, morphological alterations such as cell shrinkage, membrane blebbing, nuclear fragmentation, and chromatin condensation were observed in Hela, HepG2, and HT-29 cells [70, 74, 75]. Apoptosis is a crucial mechanism in the death of cancer cells [76], and in alignment with prior studies, our results indicate that apoptosis is the primary cause of cancer cell mortality [77, 78].

Apoptosis is induced through three primary pathways: (1) the mitochondrial pathway (intrinsic apoptotic pathway), (2) the death receptor pathway (extrinsic apoptotic pathway), and (3) the endoplasmic reticulum (ER) pathway [79]. The mitochondrial-dependent intrinsic apoptosis pathway is triggered in response to intrinsic proapoptotic stimuli like DNA damage, chemotherapeutic agents, and intracellular ROS. The intrinsic mitochondrial pathway is managed by pro and anti-apoptotic structural proteins of the B-cell lymphoma 2 (Bcl-2) family, which regulate the permeability of the mitochondrial outer membrane to proteins such as cytochrome c [80, 81]. The initiation of this pathway eventually results in the release of Bcl-2 pro-apoptotic proteins from the mitochondria, the activation of the caspase cascade, and ultimately, the induction of apoptosis. However, the Bcl-2

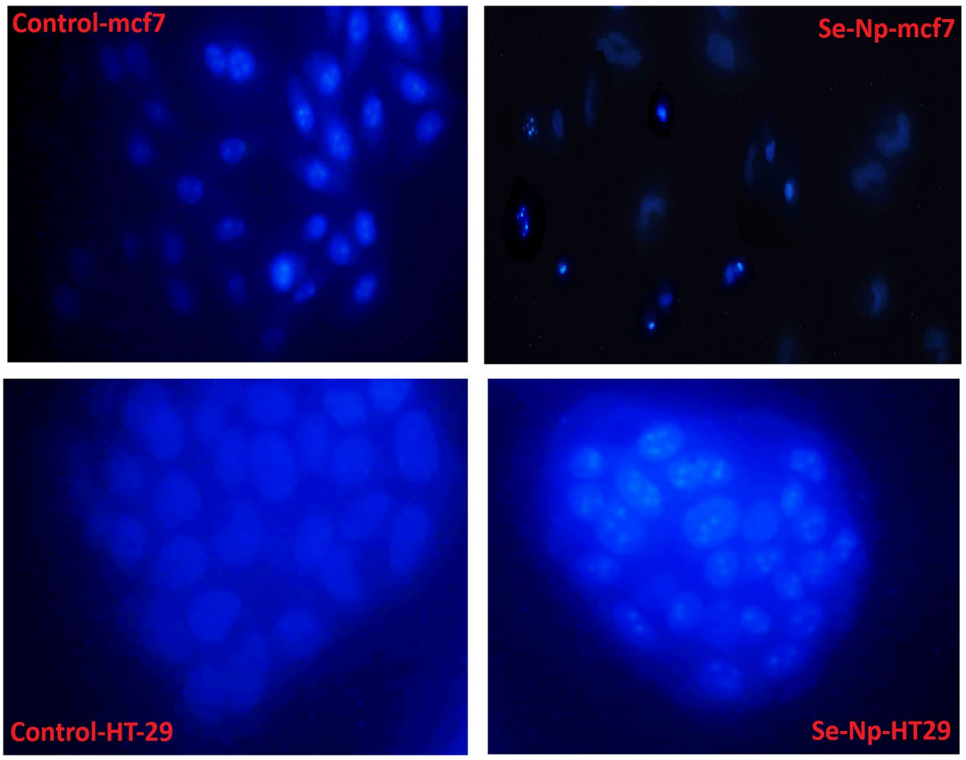

Fig. 6 DAPI staining of MCF7, HT-29, and control cells to show apoptosis induced by *LC*-SeNPs

anti-apoptotic protein hinders the release of cytochrome c from the mitochondria [80, 82].

The extrinsic or death receptor pathway induces apoptosis through the binding of death ligands (FasL, TRAIL) to their respective death receptors (TNFRSF), forming the death signaling complex (DISC), and subsequently activating caspase [80, 83]. BAX, Caspase 3, and Caspase 9 proteins, encoded by related genes, are classic proteins involved in the intrinsic pathway of apoptosis. It is well established that Caspase 9 activates Caspase 3, which is critical for the execution phase of apoptosis, and an increase in these protein levels is an indication of apoptosis [84].

The authors' hypothesis concerning the anticancer properties of SeNPs revolves around the interaction with endogenous copper, particularly copper bound to chromatin, which leads to Reactive Oxygen Species (ROS) generation. Notably, certain types of cancer exhibit higher copper levels within cells and in serum. SeNPs have the capacity to form a complex with copper bound to chromatin, consequently reducing Cu (II) to Cu (I). The reoxidation of Cu (I) then triggers substantial ROS production, which serves to effectively eliminate cancer cells [52]. Thus, SeNPs emerge as potential chemopreventive and chemotherapeutic agents against human cancers [85].

This study explored the gene expression changes in HT-29 and MCF-7 cells following treatment with *LC*-SeNPs, particularly focusing on genes linked to apoptosis induction. The qRT-PCR results revealed an increase in the expression of *BAX, CASP3*, and *CASP9* genes as compared to normal cells, indicating that *LC*-SeNPs therapy stimulates apoptosis. However, no marked decrease was noted in the expression of the *BCL2* gene, an anti-apoptotic agent, post *LC*-SeNPs treatment in both cell types. Moreover, the expression of *BAX*, *CASP3*, and *CASP9* genes in MCF-7 cells exposed to *LC*-SeNPs was significantly higher than in HT-29 cells (Fig. 7). The study by Huang et al. demonstrated that Tf-SeNPs exert a strong cytotoxic effect on cancer cells by inducing apoptosis

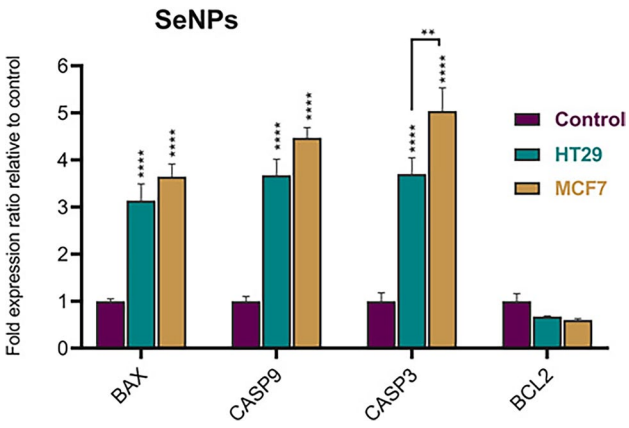

Fig. 7 The comparison of expression levels of genes responsible for apoptosis induction after 24 h of treatment with *LC-SeNPs*

through both intrinsic and extrinsic pathways [36]. Othman et al. explored the anticancer properties of SeNPs, revealing that SeNPs containing berberine can stimulate apoptosis by down-regulating *BCL2* and upregulating the expression of *BAX* and *CASP3* genes [86]. Pi et al. reported that SeNPs notably enhanced apoptosis and necrosis in MCF-7 cells compared to control cells (12.74% versus 4.27%). Additionally, the expression of key apoptosis regulatory proteins like Caspase 9 and Caspase 3 was markedly higher than in the control group [87]. Furthermore, biosynthesized black ginger-selenium nanoparticles were found to induce apoptosis by upregulating *BAX*, *Caspase 3*, and downregulating *BCL2* [88]. The anticancer properties of biosynthesized SeNPs were also reported against A549 cancer cells and human cervical cancer cells, with findings indicating a significant increase in caspase-3 activity, ROS overproduction, and mitochondrial dysfunction [51].

Collectively, these findings align with prior research results, reinforcing the concept that SeNPs possess cytotoxic effects and promote apoptosis in cancer cell lines [89, 90].

Impact of *LC*-SeNP Treatment on Cell Cycle Arrest

This study observed a hindered proliferation of HT-29 and MCF-7 cells when treated with SeNPs, resulting in cell cycle arrest in the sub-G1 phase. Cell cycle analysis revealed that *LC*-SeNPs obstructed the cell cycle, leading to sub-G1 phase arrest in both MCF-7 and HT-29 cells, which effectively inhibited cell proliferation. Consequently, the percentage of cells in the sub-G1 phase was significantly higher in HT-29 and MCF-7 cells treated with *LC*-SeNPs compared to the control group (17.69% and 25.29% vs. 0.62%, respectively). In contrast, the number of HT-29 cells in the

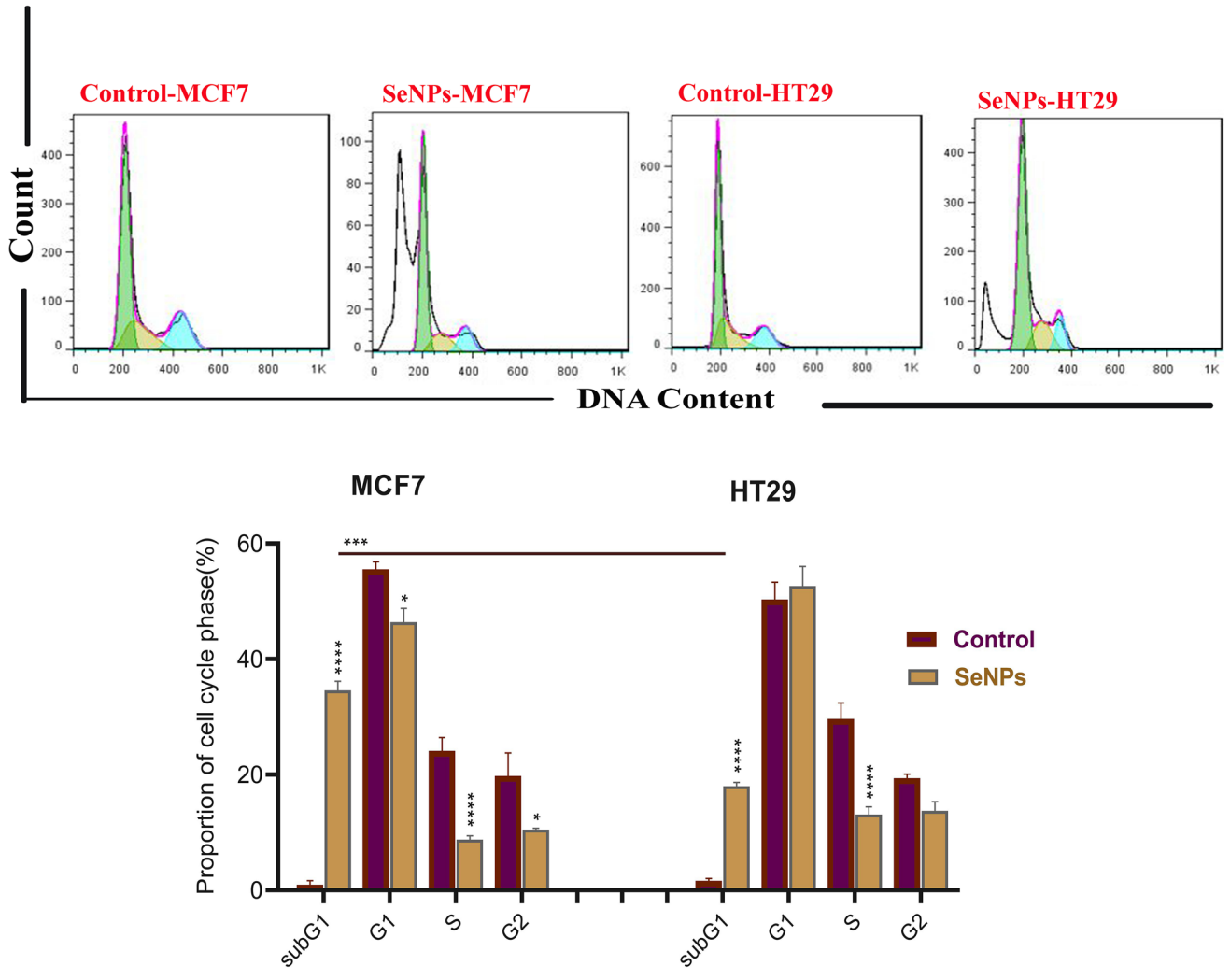

Fig. 8 Cell cycle analysis of MCF-7 and HT-29 cells treated with *LC-SeNPs* compared to the control group (****$P < 0.0001$, ***$P < 0.001$, and *$P < 0.05$)

G1 phase decreased significantly compared to the control. Additionally, the number of MCF-7 cells in the S and G2 phases showed a significant reduction compared to the control (Fig. 8). Several studies have demonstrated the impact of SeNPs on cell cycle arrest and cell death pathways in different cancer cell lines. Our findings align with these studies, as sub-G1 phase cell cycle arrest was observed, as reported in other studies as well [74, 91].

The mechanisms of cell cycle arrest and cell death can vary depending on the specific selenium compounds used and the cell phenotype [92]. SeNPs can selectively enter cancer cells through endocytosis and induce cancer cell apoptosis via signal transduction pathways [87, 93]. Conversely, various studies have reported selenite's ability to arrest the cell cycle at the S or G2/M phases [94–96]. For instance, Bidkar et al. explored SeNPs as a delivery system and demonstrated that paclitaxel-loaded SeNPs arrested cancer cells in the G2/M phase in a dose-dependent manner, resulting in a significant antiproliferative effect on A549, MCF-7, HeLa, and HT-29 cells [97]. Lopez-Heras et al. proposed that SeNPs inhibit the growth of HepG2 cells by inducing cell cycle arrest in the S phase. This effect is mediated by the re-regulation of the eIF3 protein complex, which impacts the protein synthesis machinery and inhibits cell cycle progression [98].

Uptake of *LC*-SeNPs

Figure 9A and B show fluorescence microscopy photographs of MCF-7 cells after 24 h of treatment with *LC*-SeNPs at 37 °C. It appears that the cells' fluorescence was boosted following treatment with the IC_{50} concentration of *LC*-SeNPs. The intensity of the fluorescence of the cells was monitored using a microplate reader in order to further quantify the cellular uptake efficiency of the *LC*-SeNPs (Fig. 9C). Figures also depict the cellular uptake of *LC*-SeNPs by malignant cells after 24-h incubation at the IC_{50} concentration of *LC*-SeNPs at 37 °C. When cells were treated with *LC*-SeNPs, the efficiency of cellular uptake had improved (Fig. 9). Previous studies have suggested that SeNPs have the capacity to penetrate various cell types through unique endocytosis pathways, thus eliciting toxic effects [99]. Moreover, SeNPs have exhibited greater selectivity between normal and cancer cells compared to Se^{+IV} at similar concentrations, in addition to their distinct anticancer effectiveness. Specifically, cancer cells selectively internalize SeNPs via endocytosis, which then induce cell apoptosis by activating apoptotic signal transduction pathways [87, 93]. To date, numerous studies on intracellular mechanisms have suggested that SeNPs enter cancer cells via endocytosis and trigger apoptosis of cancer cells through signal transduction pathways [36, 100, 101]

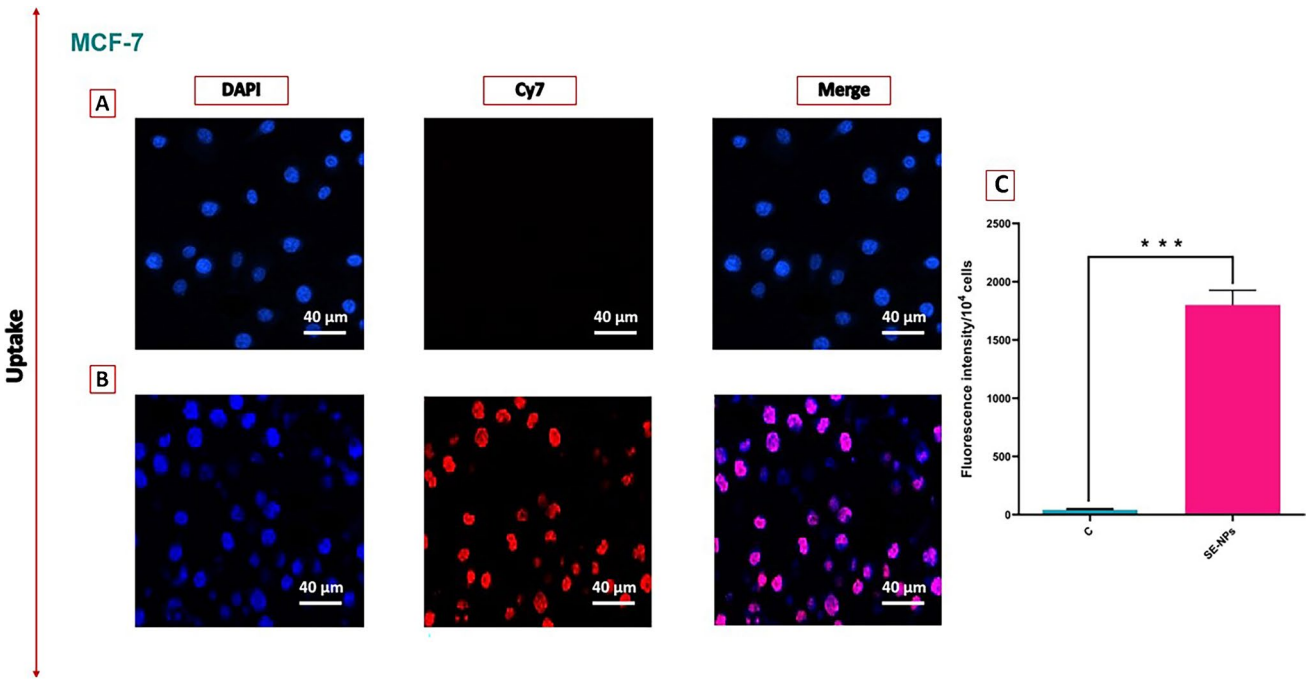

Fig. 9 Fluorescence images of MCF-7 cells after 24 h incubation with LC-SeNPs and Cy7 dye, (**A**) MCF-7 untreated cells (control) (**B**) MCF-7 cells treated with IC50 concentration of LC-SeNPs and Cy7 dye. (**C**) Quantitative analysis of cellular uptake of LC-SeNPs and Cy7 dye by MCF-7. Data represent means ± standard deviations (n=3). Significant difference specified as $^*P < 0.05$

Suppression of Migration in MCF-7 and HT-29 Cell Lines by *LC*-SeNPs

In addition to studying the impact of metal nanoparticles on cell proliferation, this research also investigated their effect on cell motility. Notably, metastasis is a critical characteristic of cancer, and approximately 90% of cancer-related deaths are attributed to metastasis [102]. Consistent with prior studies, SeNPs were found to inhibit cell migration and invasion [89]. Our data also indicate that apart from their antiproliferative effect, SeNPs have inhibitory effects on the migration of cancer cells. The scratch test was employed to examine the migration capacity of HT-29 and MCF-7 cells in the presence of selenium nanoparticles. As illustrated in Fig. 10A, 24 h after SeNP treatment, the migration rate of MCF-7 cells significantly decreased compared to the control group ($P < 0.01$). Furthermore, the scratch test revealed a significantly lower migration rate in HT-29 cells treated with *LC*-SeNPs within 24 h compared to the control group ($P < 0.05$) (Fig. 10B).

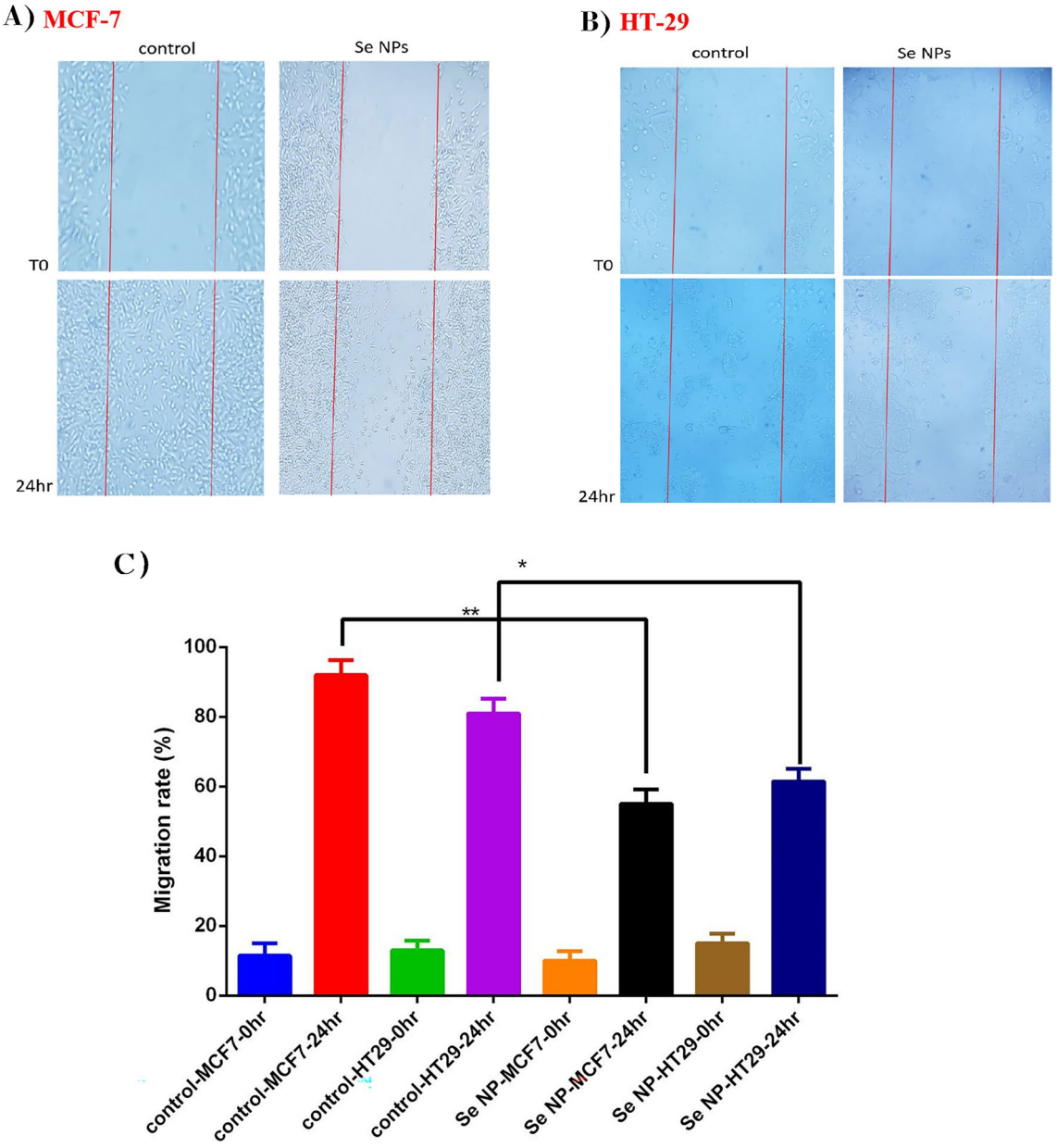

Fig. 10 The scratch test to investigate the capacity of MCF-7 (**A**) and HT-29 (**B**) cells to migrate under the presence of LC-SeNPs. The migration rate of MCF-7 (**$P < 0.01$) and HT-29 (*$P < 0.05$) cells during 24-hour treatment with LC-SeNPs compared to the control group

After 24 h, the wounds of the MCF-7 control, HT-29 control, and *LC*-SeNPs in MCF-7 and HT-29 groups showed approximately 80%, 70%, 35%, and 20% healing, respectively (Fig. 10C).

Similarly, Xia et al. reported a wound healing rate of approximately 21.9% after 24 h with SeNPs@Am treatment. The use of SeNPs@Am inhibited the aggressiveness of cancer cells [75].

Li et al. demonstrated that biologically synthesized SeNPs with Galangin significantly suppressed the migration of HepG2 cells [103].

Conclusion

In summary, this study reveals the anticancer activity of *LC*-SeNPs synthesized by *L. casei*, which inhibits the proliferation and cell cycle of HT-29 and MCF-7 cells, and induces apoptosis through the up-regulation of apoptosis-related genes. Furthermore, *LC*-SeNPs exhibit inhibitory effects on the migration of HT-29 and MCF-7 cells, providing a potential strategy to prevent the invasion of cancerous cells. These findings offer in vitro evidence supporting the anticancer and anti-metastatic effects of *LC*-SeNPs, forming a basis for further pre-clinical and clinical investigations.

Abbreviations SeNPs: Selenium nanoparticles; CFS: Cell-free supernatant; *L. casei*: *Lactobacillus casei*; *LC*-SeNPs: Green-synthesized SeNPs via the cell-free supernatant (CFS) of *Lactobacillus casei*; CRC: Colorectal cancer; Se: Selenium; ROS: Reactive oxygen species; UV-vis: Ultraviolet-visible spectroscopy; SEM: Field emission scanning electron microscopy; EDX: Energy-dispersive X-ray spectroscopy; TEM: Transmission electron microscopy; XRD: X-ray powder diffraction; FT-IR: Fourier transform infrared spectroscopy; DLS: Dynamic light scattering particle size distribution analysis; HFF: Human foreskin fibroblasts; RT: Reverse transcriptase; IC_{50}: Half maximal inhibitory concentration; DAPI: 4′,6-Diamidino-2-phenylindole dihydrochloride

Acknowledgements The authors would like to acknowledge the Cellular and Molecular Research Center, Islamic Aazad University.

Author Contribution Z. H. M. N.: data curation, formal analysis, methodology, writing — original draft. F. T.: methodology, project administration, data curation, supervision, writing — review and editing. K. A.: assisted in performing the cell culture experiments. N. KD.: assisted in performing the cell culture experiments. B. K.: assisted in performing the cell culture experiments. All authors have read and agreed to the published version of the manuscript.

Data Availability The datasets used and/or analyzed during the current study are available from the corresponding author on reasonable request.

Declarations

Competing interests The authors declare no competing interests.

Ethics Approval Not applicable.

Consent to Participate Not applicable.

Informed Consent All authors consent to the publication of this study.

Conflicts of Interest The authors declare no competing interests.

References

1. Kocarnik JM et al (2022) Cancer incidence, mortality, years of life lost, years lived with disability, and disability-adjusted life years for 29 cancer groups from 2010 to 2019: a systematic analysis for the global burden of disease study 2019. JAMA Oncol 8:420–444
2. Sung H et al (2021) Global Cancer Statistics 2020: GLOBOCAN estimates of incidence and mortality worldwide for 36 cancers in 185 countries. CA Cancer J Clin 71:209–249. https://doi.org/10.3322/caac.21660
3. Łukasiewicz S et al (2021) Breast cancer—epidemiology, risk factors, classification, prognostic markers, and current treatment strategies—an updated review. Cancers 13:4287
4. Hailu HE, Mondul AM, Rozek LS, Geleta T (2020) Descriptive epidemiology of breast and gynecological cancers among patients attending Saint Paul's Hospital Millennium Medical College, Ethiopia. PLoS ONE 15:e0230625
5. Liang S, Deng X, Ma P, Cheng Z, Lin J (2020) Recent advances in nanomaterial-assisted combinational sonodynamic cancer therapy. Adv Mater 32:2003214
6. Cordani M, Somoza Á (2019) Targeting autophagy using metallic nanoparticles: a promising strategy for cancer treatment. Cell Mol Life Sci 76:1215–1242
7. Tariq K, Ghias K (2016) Colorectal cancer carcinogenesis: a review of mechanisms. Cancer Biol Med 13:120–135. https://doi.org/10.28092/j.issn.2095-3941.2015.0103
8. Kuipers EJ et al (2015) Colorectal cancer. Nat Rev Dis Primers 1:15065. https://doi.org/10.1038/nrdp.2015.65
9. Hulla J, Sahu S, Hayes A (2015) Nanotechnology: history and future. Hum Exp Toxicol 34:1318–1321
10. Sabri MA, Umer A, Awan GH, Hassan MF, Hasnain A (2016) Selection of suitable biological method for the synthesis of silver nanoparticles. Nanomater Nanotechnol 6:29. https://doi.org/10.5772/62644
11. Dikshit PK, Kumar J, Das AK, Sadhu S, Sharma S, Singh S, Gupta PK, Kim BS (2021) Green synthesis of metallic nanoparticles: Applications and limitations. Catalysts 11(8):902
12. Mohammadi Shivyari A, Tafvizi F, Noorbazargan H (2022) Anti-cancer effects of biosynthesized zinc oxide nanoparticles using Artemisia scoparia in Huh-7 liver cancer cells. Inorg Nano-Met Chem 52:375–386
13. Ahmed S, Ikram S (2016) Biosynthesis of gold nanoparticles: a green approach. J Photochem Photobiol, B 161:141–153
14. Faramarzi MA, Sadighi A (2013) Insights into biogenic and chemical production of inorganic nanomaterials and nanostructures. Adv Coll Interface Sci 189:1–20
15. Faramarzi MA, Forootanfar H (2011) Biosynthesis and characterization of gold nanoparticles produced by laccase from Paraconiothyrium variabile. Colloids Surf, B 87:23–27
16. Yang J et al (2009) Interaction between antitumor drug and silver nanoparticles: combined fluorscence and surface enhanced Raman scattering study. Chin Opt Lett 7:894–897
17. Banerjee K, Ravishankar Rai V (2018) A review on mycosynthesis, mechanism, and characterization of silver and gold nanoparticles. BioNanoScience 8:17–31

18. Shirsat S, Kadam A, Naushad M, Mane RS (2015) Selenium nanostructures: microbial synthesis and applications. RSC Adv 5:92799–92811. https://doi.org/10.1039/C5RA17921A
19. Radomska D, Czarnomysy R, Radomski D, Bielawska A, Bielawski K (2021) Selenium as a bioactive micronutrient in the human diet and its cancer chemopreventive activity. Nutrients 13:1649
20. Drake E (2006) Cancer chemoprevention: selenium as a prooxidant, not an antioxidant. Med Hypotheses 67:318–322
21. Perumal S, Gopal Samy MV, Subramanian D (2021) Selenium nanoparticle synthesis from endangered medicinal herb (Enicostema axillare). Bioprocess Biosyst Eng 44:1853–1863
22. Böck A et al (1991) Selenocysteine: the 21st amino acid. Mol Microbiol 5:515–520
23. Hariharan S, Dharmaraj S (2020) Selenium and selenoproteins: it's role in regulation of inflammation. Inflammopharmacology 28:667–695
24. Chaudhary S, Umar A, Mehta S (2016) Selenium nanomaterials: an overview of recent developments in synthesis, properties and potential applications. Prog Mater Sci 83:270–329
25. Dawood MA et al (2021) Selenium nanoparticles as a natural antioxidant and metabolic regulator in aquaculture: a review. Antioxidants 10:1364
26. Menon S, Agarwal H, Shanmugam VK (2021) Catalytical degradation of industrial dyes using biosynthesized selenium nanoparticles and evaluating its antimicrobial activities. Sustain Environ Res 31:1–12
27. Abdel-Moneim AM, Shehata AM, Mohamed NG, Elbaz AM, Ibrahim NS (2021) Synergistic effect of Spirulina platensis and selenium nanoparticles on growth performance, serum metabolites, immune responses, and antioxidant capacity of heat-stressed broiler chickens. Biol Trace Elem Res 200(2):768–779
28. Tang S et al (2019) Construction of arabinogalactans/selenium nanoparticles composites for enhancement of the antitumor activity. Int J Biol Macromol 128:444–451
29. Iqbal MS, Abbas K, Qadir MI (2022) Synthesis, characterization and evaluation of biological properties of selenium nanoparticles from Solanum lycopersicum. Arab J Chem 15:103901
30. El-Zayat MM et al (2021) The antimicrobial, antioxidant, and anticancer activity of greenly synthesized selenium and zinc composite nanoparticles using Ephedra aphylla extract. Biomolecules 11. https://doi.org/10.3390/biom11030470
31. Kojouri GA, Jahanabadi S, Shakibaie M, Ahadi AM, Shahverdi AR (2012) Effect of selenium supplementation with sodium selenite and selenium nanoparticles on iron homeostasis and transferrin gene expression in sheep: a preliminary study. Res Vet Sci 93:275–278. https://doi.org/10.1016/j.rvsc.2011.07.029
32. Shakibaie M et al (2013) Acute and subacute toxicity of novel biogenic selenium nanoparticles in mice. Pharm Biol 51:58–63
33. Zhao S et al (2017) Redox-responsive mesoporous selenium delivery of doxorubicin targets MCF-7 cells and synergistically enhances its anti-tumor activity. Acta Biomater 54:294–306
34. Li Y et al (2013) Functionalized selenium nanoparticles with nephroprotective activity, the important roles of ROS-mediated signaling pathways. J Mater Chem B 1:6365–6372
35. Hosnedlova B, Kepinska M, Skalickova S, Fernandez C, Ruttkay-Nedecky B, Peng Q, Baron M, Melcova M, Opatrilova R, Zidkova J, Sochor J (2018) Nano-selenium and its nanomedicine applications: a critical review. Int J Nanomed 13:2107–2128
36. Huang Y et al (2013) Selective cellular uptake and induction of apoptosis of cancer-targeted selenium nanoparticles. Biomaterials 34:7106–7116
37. Wang X, Sun K, Tan Y, Wu S, Zhang J (2014) Efficacy and safety of selenium nanoparticles administered intraperitoneally for the prevention of growth of cancer cells in the peritoneal cavity. Free Radical Biol Med 72:1–10
38. Luo H, Wang F, Bai Y, Chen T, Zheng W (2012) Selenium nanoparticles inhibit the growth of HeLa and MDA-MB-231 cells through induction of S phase arrest. Colloids Surf, B 94:304–308
39. Khurana A, Tekula S, Saifi MA, Venkatesh P, Godugu C (2019) Therapeutic applications of selenium nanoparticles. Biomed Pharmacother 111:802–812
40. Xu C et al (2018) Biogenic synthesis of novel functionalized selenium nanoparticles by Lactobacillus casei ATCC 393 and its protective effects on intestinal barrier dysfunction caused by enterotoxigenic Escherichia coli K88. Front Microbiol 9:1129
41. Shahriary S, Tafvizi F, Khodarahmi P, Shaabanzadeh M (2022) Phyto-mediated synthesis of CuO nanoparticles using aqueous leaf extract of Artemisia deserti and their anticancer effects on A2780-CP cisplatin-resistant ovarian cancer cells. Biomass Conv Bioref 1–7
42. Dehghani N, Tafvizi F, Jafari P (2021) Cell cycle arrest and anticancer potential of probiotic Lactobacillus rhamnosus against HT-29 cancer cells. Bioimpacts 11(4):245–252. https://doi.org/10.34172/bi.2021.32
43. Rahimivand M, Tafvizi F, Noorbazargan H (2020) Synthesis and characterization of alginate nanocarrier encapsulating Artemisia ciniformis extract and evaluation of the cytotoxicity and apoptosis induction in AGS cell line. Int J Biol Macromol 158:338–357
44. Lalami ZA, Tafvizi F, Naseh V, Salehipour M (2022) Characterization and optimization of co-delivery Farnesol-Gingerol Niosomal formulation to enhance anticancer activities against breast cancer cells. J Drug Delivery Sci Technol 72:103371
45. Mouritzen MV, Jenssen H (2018) Optimized scratch assay for in vitro testing of cell migration with an automated optical camera. JoVE (Journal of Visualized Experiments) (138):57691
46. San Keskin NO, Akbal Vural O, Abaci S (2020) Biosynthesis of noble selenium nanoparticles from Lysinibacillus sp. NOSK for antimicrobial, antibiofilm activity, and biocompatibility. Geomicrobiol J 37:919–928
47. Ramya S, Shanmugasundaram T, Balagurunathan R (2015) Biomedical potential of actinobacterially synthesized selenium nanoparticles with special reference to anti-biofilm, anti-oxidant, wound healing, cytotoxic and anti-viral activities. J Trace Elem Med Biol 32:30–39
48. Kora AJ, Rastogi L (2016) Biomimetic synthesis of selenium nanoparticles by Pseudomonas aeruginosa ATCC 27853: an approach for conversion of selenite. J Environ Manage 181:231–236
49. Lampis S et al (2014) Delayed formation of zero-valent selenium nanoparticles by Bacillus mycoides SeITE01 as a consequence of selenite reduction under aerobic conditions. Microb Cell Fact 13:1–14
50. Zhang X, Yan H, Ma L, Zhang H, Ren DF (2020) Preparation and characterization of selenium nanoparticles decorated by Spirulina platensis polysaccharide. J Food Biochem 44:e13363
51. Cruz LY, Wang D, Liu J (2019) Biosynthesis of selenium nanoparticles, characterization and X-ray induced radiotherapy for the treatment of lung cancer with interstitial lung disease. J Photochem Photobiol, B 191:123–127
52. Ahmad MS, Yasser MM, Sholkamy EN, Ali AM, Mehanni MM (2015) Anticancer activity of biostabilized selenium nanorods synthesized by Streptomyces bikiniensis strain Ess_amA-1. Int J Nanomed 10:3389

53. El-Saadony MT et al (2021) Selenium nanoparticles from Lactobacillus paracasei HM1 capable of antagonizing animal pathogenic fungi as a new source from human breast milk. Saudi J Biol Sci 28:6782–6794
54. Dhanjal S, Cameotra SS (2010) Aerobic biogenesis of selenium nanospheres by Bacillus cereus isolated from coalmine soil. Microb Cell Fact 9:1–11
55. Mosallam FM, El-Sayyad GS, Fathy RM, El-Batal AI (2018) Biomolecules-mediated synthesis of selenium nanoparticles using Aspergillus oryzae fermented Lupin extract and gamma radiation for hindering the growth of some multidrug-resistant bacteria and pathogenic fungi. Microb Pathog 122:108–116
56. Srivastava P, Braganca JM, Kowshik M (2014) In vivo synthesis of selenium nanoparticles by Halococcus salifodinae BK18 and their anti-proliferative properties against HeLa cell line. Biotechnol Prog 30:1480–1487
57. Liao G et al (2020) Selenium nanoparticles (SeNPs) have potent antitumor activity against prostate cancer cells through the upregulation of miR-16. World J Surg Oncol 18:1–11
58. Amiri H, Hashemy SI, Sabouri Z, Javid H, Darroudi M (2021) Green synthesized selenium nanoparticles for ovarian cancer cell apoptosis. Res Chem Intermed 47:2539–2556
59. Nunes C, Mahendrasingam A, Suryanarayanan R (2005) Quantification of crystallinity in substantially amorphous materials by synchrotron X-ray powder diffractometry. Pharm Res 22:1942–1953
60. Alagesan V, Venugopal S (2019) Green synthesis of selenium nanoparticle using leaves extract of withania somnifera and its biological applications and photocatalytic activities. Bionanoscience 9:105–116
61. Hassan HU et al (2022) Comparative study of antimicrobial and antioxidant potential of olea ferruginea fruit extract and its mediated selenium nanoparticles. Molecules 27:5194
62. Ullah A et al (2021) Biosynthesis of selenium nanoparticles (via Bacillus subtilis BSN313), and their isolation, characterization, and bioactivities. Molecules 26:5559
63. Zhang W et al (2011) Biosynthesis and structural characteristics of selenium nanoparticles by Pseudomonas alcaliphila. Colloids Surf, B 88:196–201
64. Saranya T, Ramya S, Kavithaa K, Paulpandi M, Cheon YP, Harysh Winster S, Balachandar V, Narayanasamy A (2022) Green synthesis of selenium nanoparticles using solanum nigrum fruit extract and its anti-cancer efficacy against triple negative breast cancer. J Clust Sci 1–1
65. Ranjitha V, Muddegowda U, Ravishankar Rai V (2019) Potent activity of bioconjugated peptide and selenium nanoparticles against colorectal adenocarcinoma cells. Drug Dev Ind Pharm 45:1496–1505
66. Barabadi H et al (2019) Emerging theranostic biogenic silver nanomaterials for breast cancer: a systematic review. J Cluster Sci 30:259–279
67. Zhao G et al (2018) Selenium nanoparticles are more efficient than sodium selenite in producing reactive oxygen species and hyper-accumulation of selenium nanoparticles in cancer cells generates potent therapeutic effects. Free Radical Biol Med 126:55–66
68. Pi J et al (2013) Selenium nanoparticles induced membrane bio-mechanical property changes in MCF-7 cells by disturbing membrane molecules and F-actin. Bioorg Med Chem Lett 23:6296–6303
69. Tabibi M, Agaei SS, Amoozegar MA, Nazari R, Zolfaghari MR (2020) Antibacterial, antioxidant, and anticancer activities of biosynthesized selenium nanoparticles using two indigenous halophilic bacteria. Arch Hyg Sci 9:275–286
70. Ranjitha V, Ravishankar V (2018) Extracellular synthesis of selenium nanoparticles from an actinomycetes streptomyces griseoruber and evaluation of its cytotoxicity on HT-29 cell line. Pharm Nanotechnol 6:61–68
71. Wadhwani SA et al (2017) Green synthesis of selenium nanoparticles using Acinetobacter sp. SW30: optimization, characterization and its anticancer activity in breast cancer cells. Int J Nanomed 12:6841
72. Srivastava P, Kowshik M (2016) Anti-neoplastic selenium nanoparticles from Idiomarina sp. PR58–8. Enzym Microb Technol 95:192–200
73. Forootanfar H et al (2014) Antioxidant and cytotoxic effect of biologically synthesized selenium nanoparticles in comparison to selenium dioxide. J Trace Elem Med Biol 28:75–79
74. Pandey S et al (2021) Biogenic synthesis and characterization of selenium nanoparticles and their applications with special reference to antibacterial, antioxidant, anticancer and photocatalytic activity. Bioprocess Biosyst Eng 44:2679–2696
75. Xia Y, You P, Xu F, Liu J, Xing F (2015) Novel functionalized selenium nanoparticles for enhanced anti-hepatocarcinoma activity in vitro. Nanoscale Res Lett 10:1–14
76. Koren E, Fuchs Y (2021) Modes of regulated cell death in cancer modes of regulated cell death in cancer. Cancer Discov 11:245–265
77. Yazdi MH, Sepehrizadeh Z, Mahdavi M, Shahverdi AR, Faramarzi MA (2016) Metal, metalloid, and oxide nanoparticles for therapeutic and diagnostic oncology. Nano Biomed Eng 8(4)
78. Spyridopoulou K, Aindelis G, Pappa A, Chlichlia K (2021) Anticancer activity of biogenic selenium nanoparticles: apoptotic and immunogenic cell death markers in colon cancer cells. Cancers 13:5335
79. Wang J et al (2022) Role of endoplasmic reticulum stress in cadmium-induced hepatocyte apoptosis and the protective effect of quercetin. Ecotoxicol Environ Saf 241:113772
80. Ivanova D, Zhelev Z, Aoki I, Bakalova R, Higashi T (2016) Overproduction of reactive oxygen species-obligatory or not for induction of apoptosis by anticancer drugs. Chin J Cancer Res 28:383
81. Pistritto G, Trisciuoglio D, Ceci C, Garufi A, D'Orazi G (2016) Apoptosis as anticancer mechanism: function and dysfunction of its modulators and targeted therapeutic strategies. Aging (Albany NY) 8:603
82. O'Brien MA, Kirby R (2008) Apoptosis: A review of pro-apoptotic and anti-apoptotic pathways and dysregulation in disease. J Vet Emerg Crit Care 18:572–585
83. Berg D et al (2007) Enforced covalent trimerization increases the activity of the TNF ligand family members TRAIL and CD95L. Cell Death Differ 14:2021–2034
84. Slee EA, Adrain C, Martin SJ (2001) Executioner caspase-3,-6, and-7 perform distinct, non-redundant roles during the demolition phase of apoptosis. J Biol Chem 276:7320–7326
85. Zhou L et al (2022) Preparation, characterization, and antitumor activity of Chaenomeles speciosa polysaccharide-based selenium nanoparticles. Arab J Chem 15:103943
86. Othman MS et al (2022) Green-synthetized selenium nanoparticles using berberine as a promising anticancer agent. J Integr Med 20:65–72
87. Pi J et al (2013) Pathway of cytotoxicity induced by folic acid modified selenium nanoparticles in MCF-7 cells. Appl Microbiol Biotechnol 97:1051–1062
88. Wang R, Ha K-Y, Dhandapani S, Kim Y-J (2022) Biologically synthesized black ginger-selenium nanoparticle induces apoptosis and autophagy of AGS gastric cancer cells by suppressing the PI3K/Akt/mTOR signaling pathway. J Nanobiotechnol 20:1–20
89. Tian J, Wei X, Zhang W, Xu A (2020) Effects of selenium nanoparticles combined with radiotherapy on lung cancer cells. Front Bioeng Biotechnol 8:598997
90. Jiang W et al (2014) Gracilaria lemaneiformis polysaccharide as integrin-targeting surface decorator of selenium nanoparticles to achieve enhanced anticancer efficacy. ACS Appl Mater Interfaces 6:13738–13748

91. Liu W et al (2012) Selenium nanoparticles as a carrier of 5-fluorouracil to achieve anticancer synergism. ACS Nano 6:6578–6591
92. Fernandes AP, Gandin V (2015) Selenium compounds as therapeutic agents in cancer. Biochim Biophys Acta Gen Subj 1850:1642–1660
93. Zhang Y et al (2013) Enhancement of cell permeabilization apoptosis-inducing activity of selenium nanoparticles by ATP surface decoration. Nanomed: Nanotechnol Biol Med 9:74–84
94. Li Z, Meng J, Xu T, Qin X, Zhou X (2013) Sodium selenite induces apoptosis in colon cancer cells via Bax-dependent mitochondrial pathway. Eur Rev Med Pharmacol Sci 17:2166–2171
95. Jiang C, Wang Z, Ganther H, Lu J (2002) Distinct effects of methylseleninic acid versus selenite on apoptosis, cell cycle, and protein kinase pathways in DU145 human prostate cancer cells. Mol Cancer Ther 1:1059–1066
96. Shi K et al (2013) Sodium selenite alters microtubule assembly and induces apoptosis in vitro and in vivo. J Hematol Oncol 6:1–9
97. Bidkar AP, Sanpui P, Ghosh SS (2017) Efficient induction of apoptosis in cancer cells by paclitaxel-loaded selenium nanoparticles. Nanomedicine 12:2641–2651
98. Lopez-Heras I et al (2014) Effect of chitosan-stabilized selenium nanoparticles on cell cycle arrest and invasiveness in hepatocarcinoma cells revealed by quantitative proteomics. J Nanomed Nanotechnol 5:1
99. Ferro C, Florindo HF, Santos HA (2021) Selenium nanoparticles for biomedical applications: from development and characterization to therapeutics. Adv Healthcare Mater 10:2100598
100. Sonkusre P, Cameotra SS (2017) Biogenic selenium nanoparticles induce ROS-mediated necroptosis in PC-3 cancer cells through TNF activation. J Nanobiotechnol 15:1–12
101. Liu H-J et al (2020) Lentinan-functionalized selenium nanoparticles target tumor cell mitochondria via TLR4/TRAF3/MFN1 pathway. Theranostics 10:9083
102. Lu W et al (2017) Long non-coding RNA linc00673 regulated non-small cell lung cancer proliferation, migration, invasion and epithelial mesenchymal transition by sponging miR-150-5p. Mol Cancer 16:118. https://doi.org/10.1186/s12943-017-0685-9
103. Li Y et al (2018) Multifunctional selenium nanoparticles with Galangin-induced HepG2 cell apoptosis through p38 and AKT signalling pathway. R Soc Open Sci 5:180509